2026 IEEE/SICE International Symposium on System Integration (SII)
January 11-14, 2026. Cancún, México

Consideration of Materials Used in Trochoidal Gear Reducer Based on Stress Analysis of Internal Components Aimed at Weight Reduction

Hironori Satake[1] and Naoyuki Takesue[1]

Abstract— **In recent years, the demand for industrial robots has been increasing year by year and is expected to continue to grow in the future. On the other hand, efforts toward the Sustainable Development Goals (SDGs) and carbon neutrality are spreading worldwide. This paper aims to develop a lightweight reduction gear for energy-saving robots. To reduce the weight of robots, it is necessary to replace conventional metal materials with new lightweight materials. However, weight reduction generally reduces rigidity, which tends to lower the high-speed and high-precision performance required of industrial robots.**

The authors have studied the possibility of replacing metal parts with machined CFRP, POM, and 3D printer resin parts, and have examined the adaptability of these parts. In the previous report, we experimentally compared the weight, no-load running torque, torque–torsional characteristic, and dynamic torque transfer efficiency of 20 combinations of metal and resin reduction gears. In this report, we focus on the yield strength of materials and analyze the load distribution, stress of reduction gear components, taking into account the effects of assembly and fabrication errors. We then calculate and compare the output torque per volume and weight of four types of reduction gears using metal and resin combinations. Under the condition of designing within the elastic range of the materials, it was demonstrated that using resin gears could increase the maximum output while saving space and reducing weight. Additionally, the validity of the theoretical values was verified by comparing them with FEM analysis results.

I. Introduction

In recent years, the demand for industrial robots has been increasing year by year and is expected to continue to grow in the future[1]. This is due to a decrease in the working-age population, rising wages in emerging countries, and expansion of quality improvement. Conventional robots were mainly used in the manufacture of automobiles and electronic devices, but as robots themselves have become more sophisticated and less expensive, the cost of introducing them has decreased, and robots are being introduced into a variety of industries, including food, medical, and service[2], [3], [4], [5]. Furthermore, the development of cooperative robots that work side-by-side with humans in the field of industrial robotics is advancing, and the industrial robotics market is expected to expand further.

On the other hand, efforts toward the Sustainable Development Goals (SDGs) and carbon neutrality are spreading worldwide. Therefore, energy saving is also desired in industrial robots[6]. The power consumption of an industrial robot is largely related to the robot's own weight, so weight reduction can contribute to energy conservation. To reduce the weight of robots, it is necessary to replace conventional metal materials with new lightweight materials such as nonmetals, composite materials, and resins. However, weight reduction generally reduces rigidity, which tends to lower the high-speed and high-precision performance required of industrial robots.

The authors have been studying the adaptability of resin parts by replacing metal parts with parts made of materials such as machinable CFRP, POM, which is an engineering plastic, and resin materials for FDM 3D printers[7], [8], which have attracted attention in recent years, in order to reduce the weight of robots. The evaluation contents and results using metal and plastic reduction gears were presented for the development of the drive unit, which is greatly related to the power and position control performance of the robot[9], [10], [11]. In the previous report, we experimentally compared the weight, no-load running torque, torque-torsional characteristic, and dynamic torque transmission efficiency of 20 combinations of metal and resin reduction gears, and clarified the effects of the types of materials used and their combinations on the performance of the reduction gears. As a result, although the use of resin inevitably leads to a deterioration in rigidity, accuracy, and durability, it enables the reduction of weight in the reduction gear, and the deformation of the resin material that accommodates fabrication or assembly errors has been found to reduce no-load running torque and improve dynamic torque transmission efficiency. Therefore, by appropriately selecting which materials to use for which reduction gear parts, it is possible to achieve weight reduction while suppressing performance degradation compared to conventional reduction gears that use all metal.

In this paper, we focus on the yield strength of materials and analyze the load distribution, stress, and surface pressure of reduction gear components, taking into account the effects of fabrication or assembly errors. We then calculate and compare the output torque per volume and weight of four types of reduction gears using metal and resin combinations. As a result, under the condition of designing within the elastic range of the materials, it is demonstrated that using resin gears could increase the maximum output while saving space and reducing weight. Additionally, the validity of the theoretical values was verified by comparing them with FEM analysis results.

II. Trochoidal gear reducer

A. Configuration of trochoidal gear reducer

As in the previous reports [9], [10], [11], this paper treats a planetary gear reduction device using a trochoid tooth profile with an epicycloid curve [12] as the reduction

[1]Hironori Satake and Naoyuki Takesue are with Tokyo Metropolitan University, Hino, Tokyo, Japan

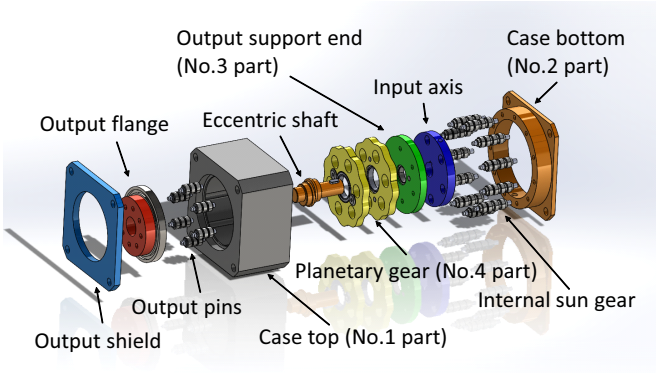

Fig. 1: Exploded view of trochoidal gear reducer parts

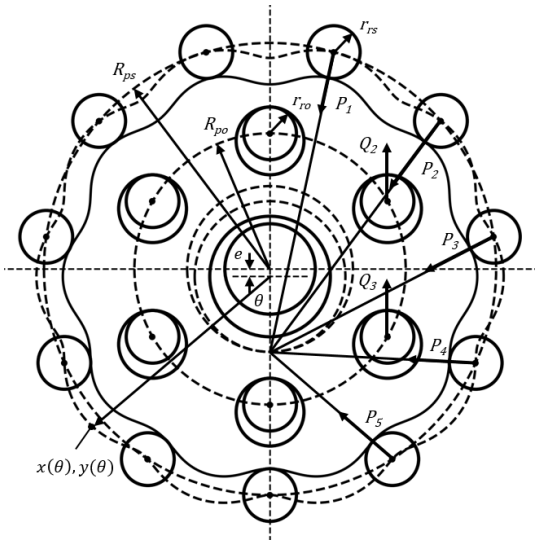

Fig. 2: Geometric model of a trochoidal gear reducer

mechanism. This reduction gear has high structural rigidity due to multiple contact points and meshing teeth, and is characterized by high efficiency due to rolling contact. In addition, the teeth have a smooth curved shape, making them easy to manufacture with a 3D printer. The internal components of the trochoidal gear reducer are shown in Fig. 1.

Figure 2 shows the geometric model of a trochoidal gear. Let θ be the angle viewed from the center of the planetary gear. Let R_{ps} be the pitch circle radius of the internal sun gear. Let e be the eccentricity from the input shaft. Let n_s be the number of teeth of the internal sun gear. The outer tooth surface of the planetary gear is a curve offset inward by the bearing radius r_{rs} of the inner sun gear from the curves represented by Eqs. (1) and (2).

$$x(\theta) = R_{ps}\cos\theta - e\cos n_s\theta \quad (1)$$

$$y(\theta) = R_{ps}\sin\theta - e\sin n_s\theta \quad (2)$$

Furthermore, let n_p be the number of teeth of the planetary gear and let N_{in} and N_{out} be the rotational speeds of the input and output shafts, respectively. Let R_{be} be the base radius and let r_{ge} be the generating radius of the epicycloid. Then, Eq. (3) holds for the reduction ratio n of the reducer.

$$\frac{1}{n} = \frac{N_{\text{out}}}{N_{\text{in}}} = \frac{r_{ge}}{R_{be}} = \frac{n_s - n_p}{n_p} = \frac{n_s}{n_p} - 1 \quad (3)$$

B. Load distribution inside trochoid gear reducer

In previous reports [9], [10], [11], the use of resin materials with lower rigidity than metals for the case top and planetary gears resulted in a reduction in no-load running torque and an improvement in dynamic torque transmission efficiency. These results are believed to be due to the material's low rigidity, which allows for deformation that accommodates geometric misalignment caused by fabrication or assembly errors. This deformation enables smooth operation. Specifically, the main three areas where resin parts are subjected to force are as follows:

1) the roller of the internal sun gear and the outer teeth of the planetary gear,
2) the output roller and the output hole of the planetary gear, and
3) the pin holes in the case top that secure the rollers of the internal sun gear.

The loads distribution on these parts are represented by the force P_i generated between the roller of the i-th ($i = 1, 2, 3, \cdots, n_s$) internal sun gear and the planetary gear, and the force Q_j generated between the j-th ($j = 1, 2, 3, \cdots, n_o$) output roller and the planetary gear. The calculation of the loads distribution on a trochoidal gear reducer is defined in [13], [14]. At this time, it is assumed that there is no loss in the reducer and that the input and output power are equal.

Let α_i be the angle between P_i and the vertical direction, l_i be the length of the moment arm of P_i, β be the input axis's rotation angle, and γ_i be the roller's position angle on the internal sun gear. Then, the following relationship holds for the instantaneous contact point between the internal sun gear and the planetary gear: Eqs. (4) to (6).

$$\alpha_i = \tan^{-1}\left[\frac{\sin n\beta + R_{ps}/R_{bs}\sin\gamma_i}{\cos n\beta - R_{ps}/R_{bs}\cos\gamma_i}\right] \quad (4)$$

$$l_i = R_{bp}\sin(\alpha_i - n\beta) \quad (5)$$

$$\gamma_i = \frac{2i-1}{n+1}\pi \quad (6)$$

where R_{bs} is the base circle radius of the internal sun gear, R_{bp} is the base circle radius of the planetary gear, and n_o is the number of output holes.

Let M_{in} and M_{out} be the input torque and the output torque of the reduction gear, respectively. The trochoidal gear reducer has two planetary gears, which are arranged at 180-degree intervals, so theoretically each gear bears half the torque. Therefore, the load on each gear is $M_a (= M_{\text{in}}/2 = M_{\text{out}}/2n)$.

$$M_a = \frac{R_{po}}{n}\sum_{j=1}^{q} Q_j\sin(\beta_j + n\beta) \quad (7)$$

$$M_a = F_b \cdot e\cos(n\beta + \varphi) \quad (8)$$

The pitch circle radius of the output roller is R_{po}, the roller radius is r_{ro}, the reaction force of the input shaft bearing is

F_b, and the angle between F_b and the horizontal plane is φ, then based on Fig. 2, it can be expressed as follows:

$$\sum_{i=1}^{p} P_i \cos\alpha_i - \sum_{j=1}^{q} Q_j \cos n\beta - F_b \sin\varphi = 0 \quad (9)$$

$$F_b \cos\varphi - \sum_{i=1}^{p} P_i \sin\alpha_i + \sum_{j=1}^{q} Q_j \sin n\beta = 0 \quad (10)$$

$$\sum_{i=1}^{p} P_i l_i - \sum_{j=1}^{q} Q_j R_{po} \sin(\beta_j + n\theta) = 0 \quad (11)$$

In the above equations,

$$p = \begin{cases} \frac{n}{2}, & \text{if } n \text{ is even,} \\ \frac{n+1}{2}, & \text{if } n \text{ is odd.} \end{cases} \quad (12)$$

and

$$q = \begin{cases} \frac{n_o}{2}, & \text{if } n_o \text{ is even,} \\ \frac{n_o-1}{2}, & \text{if } n_o \text{ is odd.} \end{cases} \quad (13)$$

Assuming that the forces P_i and Q_j are proportional to the distance from the center of rotation, Eqs. (14) and (15) hold.

$$\frac{P_i}{l_i} = \text{constant} \quad (14)$$

$$\frac{Q_j}{\sin(\beta_j + n\beta)} = \text{constant} \quad (15)$$

From Eqs. (4) to (15), P_i and Q_j are derived as in Eqs. (16) and (17), respectively.

$$P_i = \frac{M_a \sin(\alpha_i - n\beta)}{e\sum_{i=1}^{p} \sin^2(\alpha_i - n\beta)} \quad (16)$$

$$Q_j = \frac{nM_a \sin(\beta_j + n\beta)}{R_{po}\sum_{j=1}^{q} \{\sin(\beta_j + n\beta)\}^2} \quad (17)$$

What we have derived here represents the ideal contact state between the internal sun gear and the planetary gear. However, during actual production, fabrication or assembly errors may occur, preventing ideal contact from being achieved. In this paper, the load is calculated when one tooth of a planetary gear meshes with one roller of an internal sun gear, and the calculation takes into account the effects of fabrication or assembly errors.

III. Stress and Surface Pressure in Gear Reducer

Using P_i and Q_j derived in Section II-B, we derive the stress on the roller of the internal sun gear and the outer tooth surface of the planetary gear, which are the main points where the resin parts receive force, as well as the output roller and the output hole of the planetary gear, and the pin hole of the case top that fixes the roller of the internal sun gear.

A. Roller of internal sun gear and outer tooth surface of planetary gear

The roller of the internal sun gear and the outer tooth surface of the planetary gear are assumed to be in Hertzian contact. Assuming that the contacting solids are isotropic elastic bodies, the contact area is small relative to the size of the solids, there is no friction on the contacting surfaces, the surfaces are smooth with no roughness, and the deformation is within the elastic limit, Hertz's maximum contact pressure $S_{\max}$ and contact width b are given by Eqs. (18) and (19), respectively.

$$S_{\max} = \frac{2F}{\pi bL} \quad (18)$$

$$b = \sqrt{\frac{8RF}{\pi EL}} \quad (19)$$

In the above equations, E, R, F, and L are the equivalent longitudinal elastic modulus, equivalent curvature radius, load applied to the contact point, and contact length, respectively. Let the longitudinal elastic moduli of the two objects be E_1 and E_2, and the Poisson's ratios be ν_1 and ν_2. Then, Eqs. (20) and (21) are defined.

$$\frac{2}{E} = \frac{1-\nu_1^2}{E_1} + \frac{1-\nu_2^2}{E_2} \quad (20)$$

$$\frac{1}{R} = \frac{1}{R_1} + \frac{1}{R_2} \quad (21)$$

From the shear strain energy condition (Mises condition), let the shear yield stress be k and the yield stress in the short axis tensile test be σ_s.

$$k = \frac{\sigma_s}{\sqrt{3}} \quad (22)$$

In the case of line contact, $S_{\max} = 3.1k$ holds, so it is necessary to satisfy Eq. (23) in order to design within the elastic deformation range of the material.

$$\sigma_s > \frac{\sqrt{3}}{3.1} S_{\max} \quad (23)$$

The contact pressure $S_{p,i}$ between the i-th roller of the internal sun gear and the outer tooth surface of the planetary gear, the contact area b_p at that time, and the curvature radius ρ_i of the planetary gear are expressed by Eqs. (24) to (26), respectively. E_p is the Young's modulus and Poisson's ratio of the material used for the internal sun gear and planetary gear, which are substituted into Eq. (20) as E_1 and ν_1, E_2 and ν_2 in Eq. (20), and R_p is obtained by substituting the roller radius r_{rs} of the internal sun gear and the curvature radius ρ_i of the planetary gear into R_1 and R_2 in Eq. (21), respectively.

$$S_{p,i} = \frac{2P_i}{\pi b_p L} \quad (24)$$

$$b_p = \sqrt{\frac{8R_pP_i}{\pi E_p L}} \quad (25)$$

$$\rho_i = \frac{(R_{be}+r_{ge})\left[r_{ge}^2 + e^2 - 2er_{ge}\cos\left(\frac{R_{be}}{r_{ge}}\gamma_i\right)\right]^{3/2}}{r_{ge}^3 + e^2(R_{be}+r_{ge}) - er_{ge}(R_{be}+2r_{ge})\cos\left(\frac{R_{be}}{r_{ge}}\gamma_i\right)} \quad (26)$$

Therefore, the Mises stress $\sigma_{p,i}$ applied between the i-th roller of the internal sun gear and the outer tooth surface of the planetary gear is expressed by equation (27).

$$\sigma_{p,i} = \frac{\sqrt{3}}{3.1} S_{p,i} \quad (27)$$

B. Output roller and output hole of the planetary gear

The output roller and planetary gear output holes assume Hertzian contact. Therefore, as in Section III-A, we derive using equations (18)-(23). The contact pressure between the j-th output roller and the output hole of the planetary gear is denoted as $S_{q,j}$, and the contact area b_q at that time is expressed by Eqs. (28) and (29). E_q is the Young's modulus and Poisson's ratio of the materials used for the output roller and planetary gear, which are substituted into Eq. (20) as E_1 and ν_1, E_2 and ν_2 in Eq. (20), and R_p is obtained by substituting the output roller radius r_{ro} and the planetary gear curvature radius ρ_i into R_1 and R_2 in Eq. (21), respectively.

$$S_{q,j} = \frac{2Q_j}{\pi b_q L} \tag{28}$$

$$b_q = \sqrt{\frac{8R_q Q_j}{\pi E_q L}} \tag{29}$$

The Mises stress $\sigma_{q,j}$ between the j-th output roller and the output hole of the planetary gear is expressed by Eq. (27).

$$\sigma_{q,j} = \frac{\sqrt{3}}{3.1} S_{q,j} \tag{30}$$

C. Pin hole of the case top that fixes the roller of the internal sun gear

Let the depth of the pin hole be l_d and the diameter of the pin be d_p. At this time, P_i acts on two locations, Case top and Case bottom, so the approximate value of the surface pressure $S_{h,i}$ applied to the i-th pin hole of the case top that fixes the roller of the internal gear is calculated using Eq. (31).

$$S_{h,i} = \frac{P_i}{2 l_d d_p} \tag{31}$$

IV. Lightweight design of gear reducer

When resin is used in the gear reducer, resin deformation of the resin parts can prevent the reduction gear from performing as intended, leading to a decline in performance, such as durability. This paper focuses on the yield strength of materials used in reduction gears, considers the design of reduction gears within the elastic range of materials, and evaluates the space-saving and weight-reducing properties of metal and resin reduction gears.

A. Design parameters

Eqs. (27), (30), and (31) derived in Section III are used to compare the output torque per unit volume and the output torque per unit weight from the perspective of the yield stress of the materials used in trochoidal gear reducers made of metal and resin. The design parameters of the reduction gear at this time are shown in Table I.

In the previous report, the characteristics of reduction gears were compared by replacing the case top and planetary gear with metal and resin in Fig. 1. In this paper, we consider the design of four types of reduction gears using A7075 and POM for the Case top and SUS304 and POM for the planetary gear. The materials and weights used in the four material combinations are shown in Table II. The Young's module of SUS304, A7075, POM, and steel are 193, 69, 2.4, and 206 GPa, the Poisson's ratios are 0.34, 0.28, 0.3, and 0.29, respectively, and the densities are 8.03, 2.71, 1.2, and 7.9 $\times 10^3$ kg/m^3, respectively.

TABLE I: Design parameters

Symbol	Value	Symbol	Value
e	1 mm	r_{ro}	3.5 mm
n	10	r_{rs}	3.5 mm
n_o	6	L	5 mm
R_{ps}	30 mm	l_d	4 mm
R_{po}	18 mm	d_p	3 mm

TABLE II: Four combinations of materials and weights

No.	Material				Weight [g]
	Case	Gear	Pin	Bearing	
1	A7075	SUS304	Steel	SUS304	774
2	POM				711
3	A7075	POM			678
4	POM				615

B. Limit output torque of reduction gear

In Section III, Eqs. (27), (30), and (31) were derived. For each stress and surface pressure, let the largest value of $\sigma_{p,i}$ ($i = 1, \cdots, n_s$) be $\sigma_{p,\max}$, the largest value of $\sigma_{q,j}$ ($j = 1, \cdots, n_o$) be $\sigma_{q,\max}$, and the largest value of $S_{h,i}$ ($i = 1, \cdots, n_s$) be $S_{h,\max}$, respectively.

The results of calculating how these stresses and surface pressures change with respect to the output torque M_{out} for four combinations are shown in Fig. 3.

In any combination, stress and surface pressure tend to increase as output torque increases. At this time, let the yield stress of the material used for the gear be $\sigma_{y,\text{gear}}$ and the yield stress of the material used for the case be $\sigma_{y,\text{case}}$. In Fig. 3, when $\sigma_{p,i}$ and $\sigma_{q,j}$ intersect with $\sigma_{y,\text{gear}}$ or $S_{h,i}$ intersects with $\sigma_{y,\text{case}}$, the material yields, so if the safety factor is not considered, the output torque at that point can be considered the limit output torque of the reduction gear for these material combinations. In particular, the value of $\sigma_{p,\max}$ is large, and the yield strength $\sigma_{y,\text{gear}}$ of the material used for the gear is reached by an output torque that is smaller than other stresses and surface pressures. Therefore, it can be said that the yield strength of the gear material affects the limit output torque in the design parameters of this reduction gear.

C. Limit output torque per volume and weight

The limiting output torque per unit volume of the reducer is derived. Since the reducer used in this paper has the same design as that reported in [11], its external dimensions are $70 \times 70 \times 41.5$ mm, and its volume is 2.03×10^5 mm^3. Dividing the maximum output torque by the volume yields the maximum output torque per unit volume, as shown in Fig. 4.

Similarly, the limiting output torque per unit weight of the reduction gear is derived. The limiting output torque of each combination is divided by its respective weight from Table

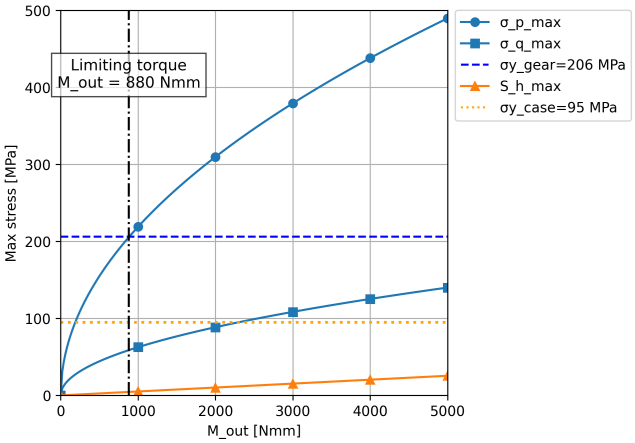

(a) Case:A7075, Gear:SUS304

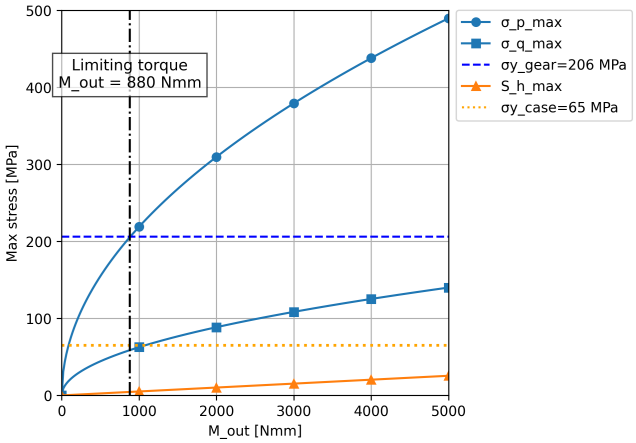

(b) Case:POM, Gear:SUS304

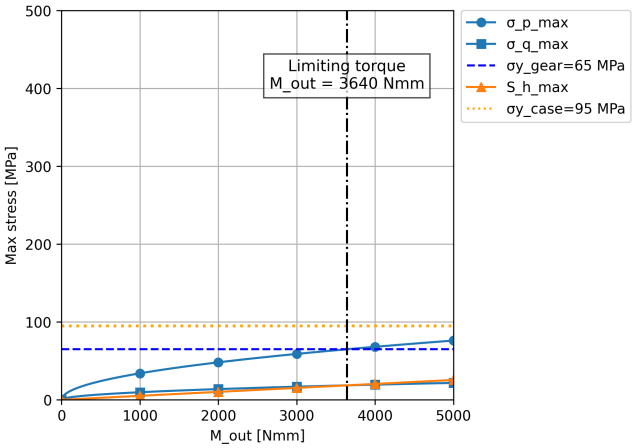

(c) Case:A7075, Gear:POM

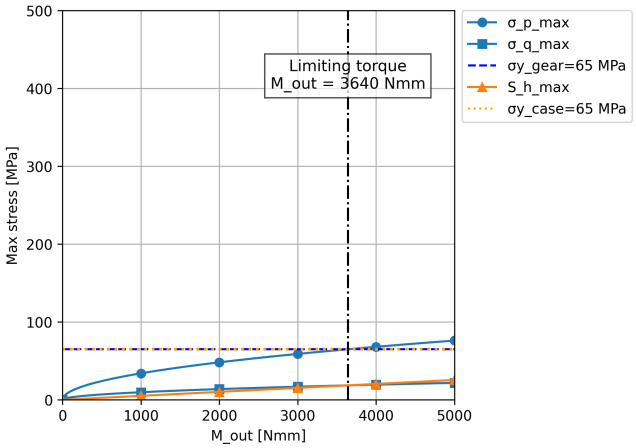

(d) Case:POM, Gear:POM

Fig. 3: Limit output torque of four types of trochoidal gear reducers

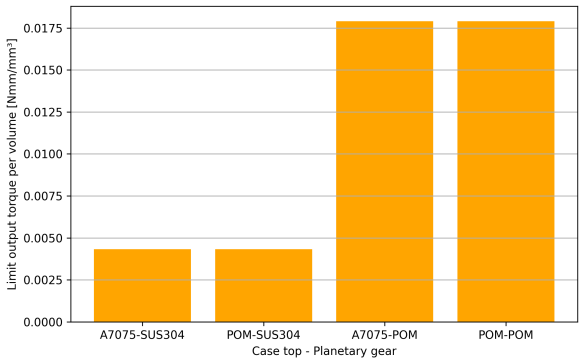

Fig. 4: Limit output torque per volume

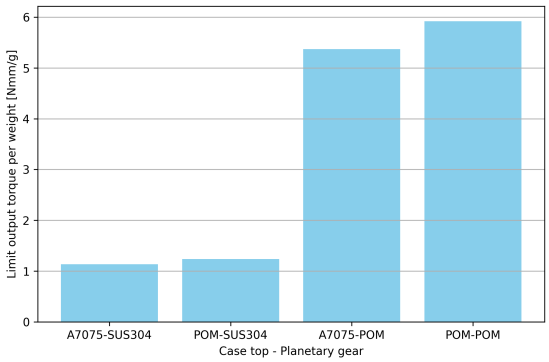

Fig. 5: Limit output torque per weight

Table II to obtain the limiting output torque per unit weight shown in Fig. 5.

Consequently, the combination using POM for the gear achieves a higher maximum output torque per unit of volume and weight than the combination using SUS304. When the gear is made of POM, its lower stiffness compared to SUS304 creates a larger contact area between the bearing and the tooth surface. This reduces stress, resulting in a higher maximum output torque based on yield stress. From a weight perspective, resin materials such as POM are less dense than metals. When designing within the material's elastic range, using resin is expected to increase maximum output torque per unit volume and weight.

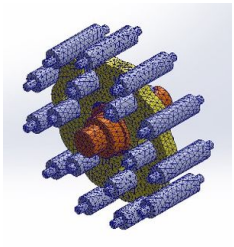

Fig. 6: FEM model (mesh size: 2 mm)

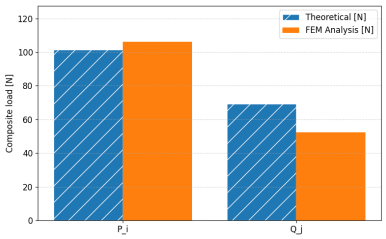

Fig. 7: Comparison of resultant forces P_i and Q_j

V. Comparison of Theoretical Values and FEM Analysis Results

To verify the validity of the analysis, we compare the theoretical values obtained based on calculations up to Section IV with the FEM analysis. The design parameters of the reduction gear are the same as those in Table I. The model was designed using SOLIDWORKS and meshed with a mesh size of 2 mm, as shown in Figure 6. FEM analysis is performed with a torque of $M_a = 0.1$ Nm applied to the input shaft of this model. The analysis uses a solid mesh and performed using Intel Direct Sparse for computation. The theoretical calculation took a few seconds, while the FEM analysis took about 10 minutes.

Comparisons between the theoretical values and FEM analysis results for the resultant forces P_i and Q_j are shown in Fig. 7. Since the results of the theoretical analysis of the force are of the same order of magnitude as the FEM analysis results, the theoretical analysis can be considered a valid guideline. However, the stress results differed significantly, though the figure is not shown here due to space limitations. The stress results varied depending on the mesh size and require further investigation in the future.

VI. Conclusion

This paper derives the loads on the gears, rollers, pins, and cases of reduction gears, taking into account fabrication or assembly errors. It also analytically derives the stresses at points considered important in the design of metal and resin reduction gears. Then, the limit output torque was calculated for each of the four types of reduction gears combining metal and resin based on the yield stress of the material. The limit output torque per volume and weight of each reduction gear was then calculated and compared. Under the condition of designing within the elastic range of the materials, it was demonstrated that using resin gears could increase the maximum output while saving space and reducing weight.

Previous reports have shown that the use of resin parts has the advantages of reducing no-load running torque and improving dynamic torque transmission efficiency, but the disadvantage is a decrease in the torsional rigidity of the reduction gear. Therefore, it will be necessary to perform rigidity analysis in the future. Furthermore, although this paper used finite element analysis to compare and verify theoretical values, the goal of this study is to evaluate the validity of the design guidelines through experiments on a manufactured reducer.

Acknowledgement

This paper is based on results obtained from a project, JPNP14004, commissioned by the New Energy and Industrial Technology Development Organization (NEDO).

We thank Prof. Gen Endo (Institute of Science Tokyo), Prof. Yusuke Ohta (Chiba Institute of Technology), and Prof. Takeshi Takaki (Hiroshima University) for their valuable comments and discussion.

References

[1] International Federation of Robotics: Global industrial robot sales doubled over the past five years, https://ifr.org/ifr-press-releases/newsglobal-industrial-robot-sales-doubled-over-the-past-five-years, (2022/8/17)

[2] H. Cheng and G. Ji: Design and implementation of a low cost 3D printed humanoid robotic platform, 2016 IEEE International Conference on Cyber Technology in Automation, Control, and Intelligent Systems (CYBER), 2016, pp. 86-91.

[3] Z. Wang, D. S. Chathuranga and S. Hirai: 3D printed soft gripper for automatic lunch box packing, 2016 IEEE International Conference on Robotics and Biomimetics (ROBIO), 2016, pp. 503-508.

[4] Y. Yamanaka, S. Katagiri, H. Nabae, K. Suzumori and G. Endo: Development of a Food Handling Soft Robot Hand Considering a High-speed Pick-and-place Task, 2020 IEEE/SICE International Symposium on System Integration (SII), 2020, pp. 87-92.

[5] Jeong IG, Khandwala YS, Kim JH, et al.: Association of Robotic-Assisted vs Laparoscopic Radical Nephrectomy With Perioperative Outcomes and Health Care Costs, 2003 to 2015. JAMA. 2017;318(16):1561–1568.

[6] K. Nonoyama, Z. Liu, T. Fujiwara, M. Alam,and T. Nishi: Energy-Efficient Robot Configuration and Motion Planning Using Genetic Algorithm and Particle Swarm Optimization, Energies Journal 2022, Volume 15, Issue 6, 2074.

[7] M. Pollák, J. Török, J. Zajac, M. Kočiško and M. Telišková: The structural design of 3D print head and execution of printing via the robotic arm ABB IRB 140, 2018 5th International Conference on Industrial Engineering and Applications (ICIEA), 2018, pp. 194-198.

[8] M. Pollák, J. Kaščak, M. Telišková, J. Tkáč: Design of the 3D Printhead with Extruder for the Implementation of 3D Printing from Plastic and Recycling by Industrial Robot, TEM Journal, Volume 8, Issue 3, pp. 709-713, ISSN 2217-8309.

[9] K. Iizuka, N. Takesue: Comparison of Characteristics of Internal Planetary Gear Reducer with Epitrochoid Curve using Metal and 3D Printed Parts, Proc. The 2023 IEEE/SICE International Symposium on System Integrations (SII 2023), pp.515-520, 2023.

[10] H. Satake, N. Takesue: Comparison of Characteristics of Cycloidal Gear Reducer using Metal, Plastic, and 3D Printed Parts, Proc. The 2024 IEEE/SICE International Symposium on System Integrations (SII 2024), pp.1531-1536, 2024.

[11] H. Satake, N. Takesue: Comparison of Characteristics of Cycloidal Gear Reducer of 20 Different Combinations of Metal and Plastic Parts, Proc. The 2025 IEEE/SICE International Symposium on System Integrations (SII 2025), pp.309-314, 2025.

[12] T. Yukawa and M. Kaneko: Mechanisms of a cyclo gear reducer with several gear ratios, 2012 Proceedings of SICE Annual Conference (SICE), 2012, pp. 2274-2279.

[13] S.K. Malhotra and M.A. Parameswaran: Analysis Of A Cycloid Speed Reducer, Mechanism and Machine Theory Vol. 18, No. 6, pp. 491-499, 1983

[14] Mirko Blagojević, Nenad Marjanović, Zorica Đorđević, Blaža Stojanović: STRESS AND STRAIN STATE OF SINGLE – STAGE CYCLOIDAL SPEED REDUCER, The 7 Th International Conference Research and Development of Mechanical Elements and Systems Irmes 2011, pp553-558

[15] H. Kanazawa, H. Nabae, K. Suzumori and G. Endo: Mechanical Parts Manufactured by a 3D Printer for Industrial Robot -Part1 : Measuring the accuracy of the hole shape-, Proceedings of the 2021 JSME Conference on Robotics and Mechatronics 2P3-A08.(in Japanese)